Egypt.J.Chem. **Vol. 63**, No. 3. pp. 907-919 (2020)

Egyptian Journal of Chemistry
http://ejchem.journals.ekb.eg/

Corrosion Behaviour of Copper– nickel Alloys in LiBr Solutions: A Comparative Study

Shaimaa Esmat Abd El hamid[1], Abeer Esmat El Meleigy[1], Adel Attia[1], Ali Abd El Fattah El Warraky[1*], Saad M. Abd-El-Wahab[2]

[1] Department of Physical Chemistry, National Research Center, Giza, Egypt.
[2] Physical Chemistry Department, Faculty of Science, Ain Shams University, Abbasia, Cairo, Egypt.

THE ANODIC potentiodynamic cyclic polarization behavior of Cu/10 Ni and Cu/30 Ni alloys in different wide range of LiBr concentrations from 10^{-1} to 9 M was investigated. The results obtained showed that the breakdown potential, hysteresis loop area and passive current were recorded at higher value of potentials in case of Cu/10 Ni in comparison with Cu/30 Ni. The current density showed higher values during the first few moment of polarization of both alloys studied as result of the changes the taking place on the surface. At $5x10^{-1}$ M of LiBr, in case of Cu/10 Ni, two breakdown potentials yielded two hysteresis loops, one of them was at 700 mV and the second was at more anodic potential. These are not recorded in case of Cu/30 Ni where pitting corrosion was manifested at 2 and 4 M LiBr only. The current – time measurement and surface examination of the electrode in case of Cu/30 Ni at $3x10^{-1}$ and $5x10^{-1}$M LiBr showed that the film formed at low anodic potential of 150 mV clarify the formation of small number of initiated pits which are surrounded by a passive and protective film of doped Cu_2O and the surface shown enrichment of Ni. While at all the potential studied for the Cu/10 Ni and Cu/30 Ni the surface of the alloy suffered from denickelification.

Keywords: Absorption-refrigeration systems, Corrosion, Cu/10 Ni, Cu/30 Ni, Lithium bromide, Surface analysis.

Introduction

Most of vapor compression refrigeration systems (VCRS) utilize chlorofluorocarbons (CFCs) and hydrochloroflurocarbons (HCFCs) refrigerants for their thermophysical properties. These types of chemicals were blamed for the depleted ozone layer where the chlorine in their structure reacts with ozone and destroy the atmospheric ozone layer. Montreal and Kyoto protocols [1, 2] the use of CFCs while HCFCs will be gradually banned globally by 2040. Consequently, refrigeration absorption machines (RAM) were considered again as alternative to the VCRS.

In RAM, many absorbent fluids were reported such as aqueous solutions of $CaCl_2$, $ZnCl_2$, ZnBr, alkali nitrates, alkali thiocyanates, alkali hydroxides and LiBr [3]. LiBr-H_2O is considered due to its encouraging properties such as its high hydration heat, good thermal stability, low viscosity, and lack of crystallization problems at normal working temperatures [4]. However, LiBr is corrosive to many metals and alloys in the RAM which are attributed to the aggressiveness of the bromide ions similar to that of chloride ions [5]. For this reason, it is very important to mitigate the corrosion problems either by selecting the suitable metal or alloys components in the absorption machines systems, applying corrosion inhibitors, by applying both or other appropriate methods.

Different metals and alloys were investigated for the RAM included for example stainless steel [4, 6, 7], carbon steel [4, 8-10], mild steel [11], titanium [4, 12, 13], with a special interest to copper and copper alloys because of their properties such as electrical, thermal, mechanical and corrosion resistance. Hence, it is not surprising that materials used for tubing (e.g., in condensers, evaporators), shells or reservoirs in

*Corresponding author e-mail: el_warraky@yahoo.com
Received 22/7/2019; Accepted 1/8/2019
DOI: 10.21608/ejchem.2019.14884.1916

such systems are constructed mainly from copper and their alloys.

Copper and copper– based alloys formed a large group of important construction materials used in a wide variety of areas due to their mechanical and physical properties as well as their inherent resistance to atmospheric corrosion [14, 15]. Copper-nickel alloys (also known as cupronickels) have been used for over 50 years for seawater piping and heat exchangers in many different industries because of their good resistance to generalized and localized corrosion [16, 17].

Cu-Ni is preferred in sea water applications because of its resistance to bio-fouling that is a result from the action of a low level of steady discharge of cupric ions [18, 19]. The corrosion resistance of Cu-Ni alloy is attributed to a protective layer consisted mainly of a thin strongly adherent inner barrier Cu_2O layer which is in contact with a solution through porous and thick outer Cu(II) hydroxide/oxide layer [20-22].

To date, the research on copper and copper alloys in LiBr-H_2O for RAM has focused on materials such as copper [5, 23], brass [24, 25], α-Al-bronze [26], Cu-Zn alloys [27, 28] and Cu-Ni alloy [29-31]. Some other research focused on galvanic coupling of copper and their alloys to other metals or alloys in LiBr aqueous solution [32-35].

Crystallization of LiBr-H_2O is considered as a serious problem if it happens at operation of the RAM. This crystallization tends to occur at fair concentrations especially when the absorber is air cooled. To the best of authors' knowledge, there is no systematic investigation on the effect of concentration of LiBr-H_2O on the corrosion of copper and copper alloys, instead; some limited concentrations of LiBr-H_2O have been studied on copper corrosion [5, 23, 36, 37].

The present work aimed at comparing systematically different wide range of concentrations of aqueous solutions of LiBr on the corrosion properties of Cu/10 Ni and Cu/30 Ni and the surface properties of these alloys.

Experimental

Samples were cut from Cu/10 Ni and Cu/30 Ni sheets in a form of coupons so that the area exposed to the electrolytic solution is 1 cm^2. Prior to anodic potentiodynamic cyclic polarization measurements, the surfaces of samples were abraded with emery papers of increasing fineness down to 1000 grit. Thereafter, the electrodes were washed with bidistilled water, degreased with acetone and then were re-washed with bidistilled water prior to use. The electrochemical measurements were carried out with a PS6 Meinsberger Potentiostat/Galvanostat, Germany.

Anodic potentiodynamic cyclic polarization curves were recorded in different concentrations of aqueous LiBr solution. Before polarization measurements, the sample was kept at -600 mV versus saturated calomel electrode (SCE) for 20 min. in the test solution to reduce the premier ion oxides film on the sample surface. The anodic potentiodynamic cyclic polarization test was carried out by scanning the potential of the electrode from – 600 mV towards noble values up to 2000 mV using a scanning rate of 1 mV/s and reversed again to the backward direction at the same scan rate.

Chronoamperometry measurements were performed by applying constant potential values for a certain period of time (around 120 min). Before surface analysis by scaning electron microscope (SEM) and energy dispersive X-ray (EDX), samples were taken, cleaned in bidistilled water in ultrasonic bath for ultra some cleaning of the sample for 30 min., dried between fibreless tissues and then introduced immediately into the vacuum chamber of SEM (JXA-840A electron probe microanalyzer), JEOL. SEM equipped with EDX, JXA-840A Electron probe microanalyzer, JEOL were used to analyze the composition of the samples taken.

Results and Discussion

Cyclic potentiodynamic polarization

The anodic potentiodynamic cyclic polarization curves of Cu/10 Ni and Cu/30 Ni in different concentrations of LiBr from 10^{-1} up to 9 M are shown in Fig. 1, 2. It is obvious from these two figures that after the cathodic branch the curves show an active region which is followed by a plateau region. The active region is controlled by a charge transfer reaction where the current density increased as the potential increased while the plateau of current is due to a diffusion limiting rate of cations through the film formed on the surface [38]. Figures 1, 2 depicted that the corrosion potential shifted towards more negative values as increasing LiBr concentration, which is occurred because of increasing the aggressiveness

of the medium, i.e., the increase of Br^- anions concentrations. On the other hand, two anodic peaks appeared [38] which were assigned by the symbols P_1 and P_2, this appearance was at ≤ 5x 10^{-1} M LiBr where the first peak is assigned to the first electro-oxidation of Cu metal to Cu(I) while the second peak is assigned to second electro-oxidation of Cu(I) to Cu(II). P_1 and P_2 were very sharp up to 5x10^{-1} M as represented in Fig. 3.

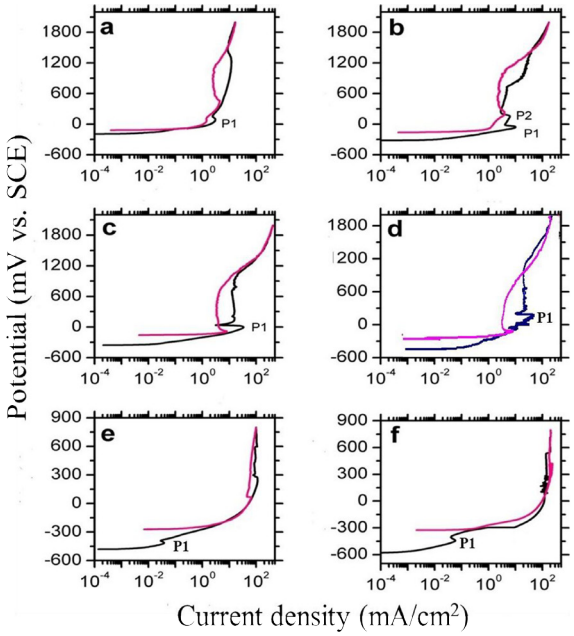

Fig. 1. Anodic potentiodynamic cyclic polarization of Cu/10 Ni in different concentrations of aqueous LiBr solution of 0.1 M (a), 1 M (b), 2 M (c), 4 M (d), 6 M (e) and 9 M (f). All potentials measured against SCE and at scan rate of 1 mV/s.

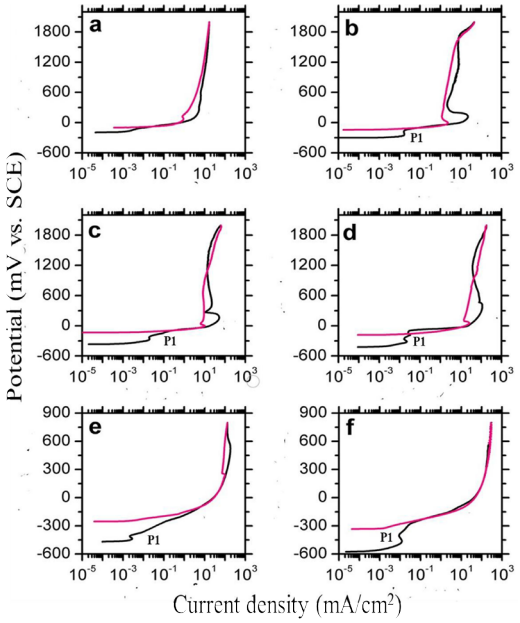

Fig. 2. Anodic potentiodynamic cyclic polarization of Cu/30 Ni in different concentration of aqueous LiBr solution of 10-1 M (a), 1 M (b), 2 M (c), 4 M (d), 6 M (e) and 9 M (f). All potentials measured against SCE and at scan rate of 1 mV/s.

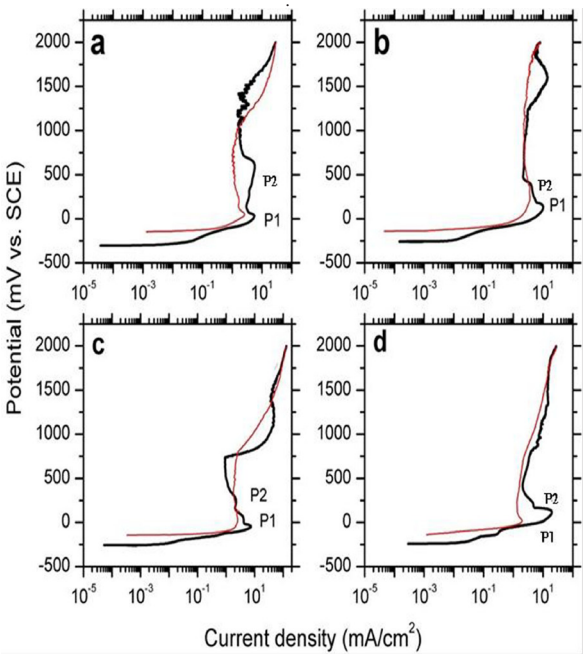

Fig. 3. Anodic potentiodynamic cyclic polarization of Cu/10 Ni and Cu/30 Ni in 3x10-1 M LiBr (a, b) and in 5x10^{-1} M LiBr (c, d), black thick line is the forward scan while the red thin line is backward scan. All scan rates were at 1 mV/s.

The anodic reaction that occurs at such concentrations may be represented by the following Eqns.

$$Cu \rightleftharpoons Cu^{+} + e^{-} \quad (1)$$

$$Cu^{+} + Br^{-} \rightleftharpoons CuBr \quad (2)$$

$$2CuBr + H_2O \rightleftharpoons Cu_2O + 2H^{+} + 2Br^{-} \quad (3)$$

$$Cu_2O + 2OH^{-} \rightleftharpoons 2CuO + H_2O + 2e^{-} \quad (4)$$

$$Cu_2O + 3H_2O \rightleftharpoons 2Cu(OH)_2 + 2H^{+} + 2e^{-} \quad (5)$$

While the cathodic reaction occurs on the cathodic site by the reduction of oxygen as:

$$O_2 + 2H_2O + 4e^{-} \rightleftharpoons 4OH^{-} \quad (6)$$

Accordingly, it is possible to conclude that P_1 appearance is due to the formation of CuBr and Cu_2O as shown in Eqns. 2 and 3, while P_2 formation is due to the oxidation of Cu_2O to higher oxidation state, i.e., to CuO and or $Cu(OH)_2$ as represented by Eqns. 4 and 5. Increasing the concentration of LiBr to ≥ 1 M, as shown in Figs. 1 and 2, resulted in the disappearance of P_2. This occurred as a result of the deleterious effect of bromide anion on the formed copper oxide to loss its passivity easily as soluble bromo-complex [37] through the formation of one or more of the reactions as described below [23, 37, 39, 40]:

$$CuBr + Br^{-} \rightleftharpoons CuBr_2^{-} \quad (7)$$

$$Cu + Br^{-} \rightleftharpoons CuBr + e^{-} \quad (8)$$

$$Cu_2O + 2H^{+} + 2Br^{-} \rightleftharpoons 2CuBr + H_2O \quad (9)$$

$$CuBr + Br^{-} + 2H_2O \rightleftharpoons CuBr_2^{-}.2H_2O + e^{-} \quad (10)$$

$$2Cu^{+} \rightleftharpoons Cu^{2+} + Cu^{0} \quad (11)$$

Equation 11 represents autocatalytic reaction or disproportionation reaction [23, 39, 40] which is defined as the presence of oxidation and reduction simultaneously, in this Eqn., Cu(I) is oxidized to form Cu(II) and at the same time it is reduced to form metallic copper.

The second reason for the disappearance of P_2 is attributed to the increase in LiBr conc., this was reported earlier for pure copper [41] when the concentration reached 1 M or higher, Cu(I) oxidation to Cu(II) is retarded on one hand and the dissolution of Cu(I) increased through the di-bromocuprate complex on the other hand as shown in Eqns. 7, 10.

Different features were depicted in Figs. 1, 2 and data summarized in Table 1: (1) As the concentration of LiBr increased for both alloys, the corrosion potential (E_{corr}), the corrosion current (I_{corr}) and the anodic current maximum peak (I_{max}) were proportionally increased; (2) In general, the passive current, the breakdown potential and the hysteresis loop started to appear at 10^{-1} M of LiBr where they disappeared after increasing the concentration to 1 M in case of Cu/10 Ni while for Cu/30 Ni started to appear at 2 M which disappeared at 6 M; (3) The range of breakdown potential, hysteresis loop, and passivity were observed at higher potential values in case of Cu/10 Ni in comparison with Cu/30 Ni alloy; (4) The current densities recorded at the passive region, which is partially passive current, from 2 to 5 $mA.cm^{-2}$ is higher than that reported previously for Cu which is nearly 0.4 $mA.cm^{-2}$ [23]. This occurred because of the dissolution of the minor element (dealloying); (5) The last important feature is presented in Fig. 3c, where for Cu/30 Ni there are two clear breakdown potentials which yielded two hysteresis loops, the first one is observed at 700 mV while the second one was observed at more anodic potential. This is not recorded in case of Cu/30 Ni.

Further insight into the alloys dissolution and oxidation in aqueous solutions could be gained from the Pourbaix diagram. Pourbaix diagram provide a thermodynamic basis for a more understanding of metal dissolution and oxide film formation in aqueous solutions at different electrochemical conditions. The immunity region of the diagram defines the potential and pH conditions where the metal does not corrode in aqueous solution. The vertical constant pH divides the corrosion and passivation regions of the diagram aqueous equilibria for M-H_2O system at 25ºC are presented in Fig. 4, where M represent metal species, in our case it is either Cu or Ni. Established procedure [37] was used to calculate the chemical and electrochemical equilibria from the free energy data. Regions of stability of metals and soluble metal species are defined depending on standard free energy data.

It is clear from the Pourbaix diagrams of Fig. 4 that Cu formed the most stable specie than Ni where the later is more active. The polarization curves of Figs. 1, 2 are nearly similar to that reported for Cu metal [38] except from 10^{-1} up to $5x10^{-1}$ M in case of Cu/10 Ni and 2 to 4 M in case of Cu/30 Ni where the corrosion potential is nearly close to each other for one and the same concentration of LiBr. Above $E_{Corr.}$, there is a region of active dissolution with an apparent Tafel slop

of △E/△log i of 60 mV [37]. The potential of this active dissolution is consistent with the formation of $CuBr^-$ complex as compared with aqueous Cu–Br-H_2O equilibria in Pourbaix diagram [37] of Fig. 4a. After that the first oxidation peak is appeared as a result to the equilibrium potential for CuBr formation as shown above in Eqn. 8.

At diluted concentration ≤ 10^{-2} and ≥ 1M LiBr, the increase in the current during the plateau region by potential may be attributed to the presence of weakly passivating CuBr salt film. This is confirmed with the observed formation of loosely adherent corrosion product with a greenish coloration on the sample surface during the experiment. This behavior is very similar to that previously reported and confirmed by using XPS technique [43, 44]. On the other hand, at concentrated solution of LiBr ≥ 1 M, another autocatalytic dissolution can take place as described by Eqn. 11 [38, 43, 44].

Equation 11 showed that Cu^{2+} is the predominant soluble species above ≈ 600 mV as shown in Figs. (1, 2) from b to f. At this potential a higher dissolution is consistent with the formation of Cu^{2+} soluble species when compared to that in Pourbaix diagram [37].

In case of Cu/10 Ni shown in of Fig. 3a at 3x10^{-1} M LiBr, P1 was formed at 50 mV while P2 was recorded at 630 mV which is followed by a sharp decrease in the current density due to the formation of a higher oxidation state (oxide or hydroxide) as described above by Eqns. 4 and 5, respectively.

The formed film is attacked by Br^- through pitting corrosion where $E_{pit.}$ is recorded at 1400 mV vs SCE and $E_{rp.}$ at 1050 mV vs SCE, which is occurred as a result of accumulation of corrosion products. These results represent that before the potential of the second peak (E_{p2}) general dissolution takes place whereas after E_{p2} pitting corrosion occurs. This type of pitting corrosion was detected previously in case of Cu/ 30Ni [30]. Increasing the conc. of LiBr to 5x 10^{-1} M as shown in Fig. 3c recorded that E_{p1} and E_{p2} are shifted to less positive value and the appearance of two hysteresis loops area and two types of pitting where the first one is recorded after the formation of P_1 and P_2 at $E_{pit.}$ = 700 mV vs SCE and Erp. ≈ 300 mV vs SCE. This type is recorded in case of Cu [23] while second type of pitting was recorded at more positive potential of Epit. = 1400 mV vs SCE which is the same recorded at 3x10^{-1} M LiBr of Fig. 3a.

Figs. 3b, 3d represent the anodic cyclic polarization curves of Cu/30 Ni in 3x 10^{-1} and 5 x10^{-1} M LiBr respectively. The curves of these figures represent the formation of P1 and a partial passive film was observed and there is no any type of local attack observed according to anodic cyclic polarization experiments, on the other hand, pitting corrosion was manifested at 2 and 4 M LiBr only, as shown in Fig. 2.

TABLE 1. Comparison between corrosion parameters for Cu/10 Ni and Cu/30 Ni in different concentrations of LiBr solutions

Conc. (M)	Cu/10 Ni	Cu/30 Ni	Cu/10 Ni	Cu/30 Ni	Cu/10 Ni	Cu/30 Ni	Cu/10 Ni	Cu/30 Ni	Cu/10 Ni	Cu/30 Ni	Cu/10 Ni	Cu/30 Ni	Cu/10 Ni	Cu/30 Ni
	$E_{Corr.}$ (mV)		$I_{Corr.}$ (mA.cm²)		$I_{Max.}$ (mA.cm²)		$E_{break.}$ (mV)		$E_{Prot.}$ (mV)		$E_{break.} - E_{Prot.}$ (mV)		$E_{break.} - E_{Corr}$ (mV)	
10^{-1}	-200	-200	0.7	0.45	4	-	1600	-	1550	-	50	-	1800	-
3x10^{-1}	-300	-250	1	2	8	9.817	1400	1280	1050	-	350	-	1700	1530
5x10^{-1}	-250	-250	2	2	9	18.27	700 1400	1850	300 1370	1800	400 30	50	950 1650	2100
1	-315	-300	2	3	10	19.57	1500	1780	1475	1670	25	110	1815	2080
2	-350	-390	5	5	35	75	-	1600	1010	1060	-	540	-	1990
4	-400	-420	20	10	70	120	800	1200	-	925	-	275	1200	1620
6	-490	-480	35	1	130	150	-	-	-	-	-	-	-	-
9	-590	-600	8	0.7	0.04	150	-	-	-	-	-	-	-	-

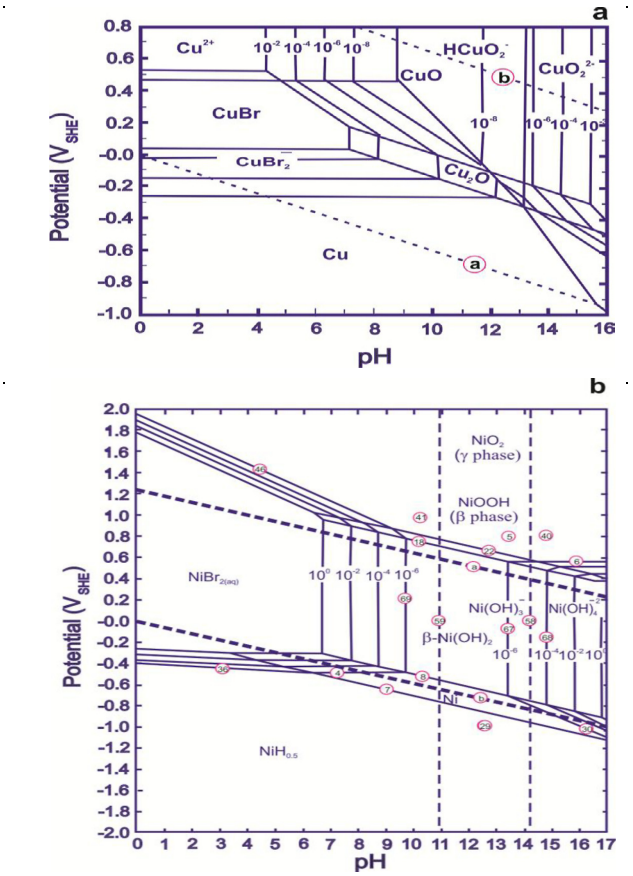

Fig. 4. Pourbaix diagram of (a) Cu-Br$^-$-H$_2$O [37] and (b) of Ni-Br$^-$-H$_2$O system at 25°C in 400 g/L LiBr [42].

Chronoamperometric measurements and surface examination

For Cu/10 Ni in 5x10^{-1} M, at 300 mV (Before breakdown potential)

Figure 5 displays that the variation of current density with time after applying a constant potential of 300 and 900 mV (curve a and b). These potentials selected as representation of before and after the breakdown potential respectively on the Cu/10 Ni in 5 x10^{-1} M LiBr. The current-time curve of Fig. 5a indicated that there is a drop in the current values during the first moment of polarization which is followed by a sluggish decrease to reach a steady state value of about 2 mA.cm^{-2} after around five min. This behavior confirmed the formation of a protective film of doped CuO [30] as shown previously in polarization curve of Fig. 3.

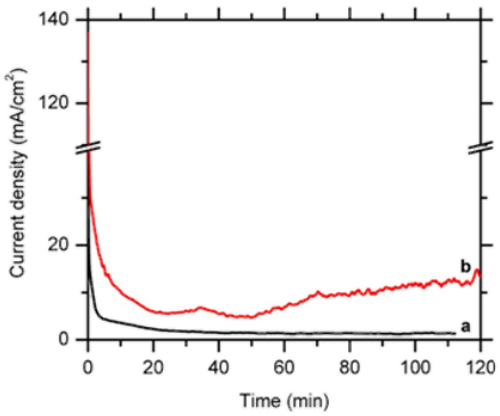

Fig. 5 Chronoamperometry of Cu/10 Ni in 5 x10^{-1} M LiBr at different constant potentials of 300 mV (a) and at 900 mV (b) [All potentials measured against SCE].

The examination of the surface of Cu/10 Ni alloy after the current-time measurements of Fig. 5 is shown in Fig. 6a, 6b; where Fig. 6a was taken at lower magnification (500x) while Fig. 6b at higher magnification (4000x). The micrograph of this figure showed that the surface was covered with a non-porous and nearly homogeneous protective film.

Examination of the surface using EDX analysis as shown in Fig. 6c indicate that oxygen and copper are detected with higher ratio of 25.17 and 67%, respectively and the detection of Br with lower ratio of 2.56 on the surface which confirm that the film formed is copper oxide. While the ratio of Cu/Ni is 12.71 which is higher than the ratio of the substrate. This means that the surface suffered from denicklification.

For Cu/10 Ni at 900 mV (after breakdown potential)

The current-time curve of Fig. 5b represents the variation of current with time at constant potential of 900 mV vs SCE. The curve shows a sharp decrease in the current density from 140 to ≈ 5 mA/cm^2 within 20 min and after that a slightly increase in the current is occur again from 5 to 12 mA/cm^2 at the end of the experiment. The increase in the current is associated with different oscillation and fluctuation. This occurs as a result of pitting corrosion. SEM examination and EDX analysis of the treated sample at the end of experiment of Fig. 5b are shown in Fig. 7a, b. The photograph of the Fig. 7a represented that the surface was covered with continuous adherent black color where some initiation and propagation of pitting are produced. The surface analysis using EDX technique of Fig. 7b shows that the atomic concentration percentage of O, Br, Ni, and Cu are 25.87, 2.89, 3.41 and 67.83 respectively. This confirm that the film formed is CuO and or $Cu(OH)_2$ and the surface of the alloy suffered from denickelification where the ratio of Cu/Ni on the film become 19.89 which is higher than that of the substrate.

For Cu/10 Ni in 3x 10^{-1} M

In the light of the above studies of anodic potentiodynamic cyclic polarization, it is necessary to study the variation of current density versus time at different constant potential of 150, 800 and 1600 mV. These values were chosen from the polarization curve of Fig. 3b for Cu/30 Ni in 3x10^{-1} M LiBr. The first curve studied at a constant potential of 150 mV represented the first peak or $I_{Max.}$ while that at constant potential of 800 mV represented a partial passive region and the third constant potential of 1600 mV was chosen to explain what happened after the breakdown potential. The current-time curves at constant potential of Fig. 8 have a general features which indicated the drop in the current values during the first moments of polarization before the current reached a quasi-stationary state depending on the applied constant potentials.

The decrease in the current detected can be reasonably be related to the changes taking place on the alloy surface. These changes arose from the formation of a doped Cu_2O film [30] that involved surface enrichment of nickel at 150 mV as confirmed later using EDX technique. The film formed at low anodic potential doped Cu_2O became a barrier that can restrict the electrolyte contact with the alloy surface, hence; the chronoamperometric measurements of Fig. 8a showed a very stable low current density value of 1.44 mA.cm^{-2} after 20 min. The SEM of Fig. 9a showed the formation of a small number of initiated pits which is surrounded by passive and protective film as confirmed from the photograph at higher magnification of Fig. 9b. EDX analysis was another evidence that support the formation of doped Cu_2O protective film as shown in Fig. 9c, where Cu was detected with lower ratio of 51.85 and Ni with higher ratio of 25.23 where Cu-Ni ratio is 2.055 which are lower than that of the alloy matrix of 2.33 which confirm the enrichment of Ni on the alloy surface. On the other hand, the detection of O with higher ratio of 20.01% in comparison with Br of 2.91% confirm the presence of Cu_2O red color film which is passive and protective enough to prevent any general dissolution and the pitting attack is occurred at very small locations.

By increasing the applied potential to 800 mV, that represent the partial passive region of Fig. 3b, the chronoamperometric feature of Fig. 8b showed a higher current density in comparison with that occur at 150 mV (Fig. 8a), which confirmed that the film formed at 800 mV is not completely protective. The SEM examination of Fig. 10a confirmed the presence of porous film and that the surface is free from any pitting attack while a general dissolution existed which confirm the region of partial passive current of Fig. 8b. Another confirmation was evidenced from the EDX analysis of Fig. 10c which represented a higher atomic % of Br of 30.71% compared to 19.35% of O while it was 42.76% for Cu and 7.18% for Ni. This meant that the film formed is $Cu_2(OH)_3Br$ as confirmed previously [30]. The ratio of Cu-Ni in the formed film is equal 5.95 which satisfy the denicklification phenomenon.

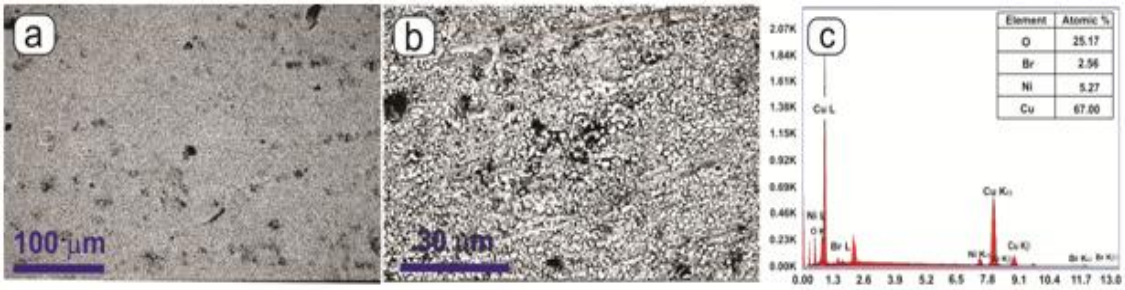

Fig. 6 SEM at 1000x (a), 4000x (b) and EDX after treated Cu/10 Ni in 5 x10^{-1} M LiBr at constant potential of 300 mV (SCE) for 120 min.

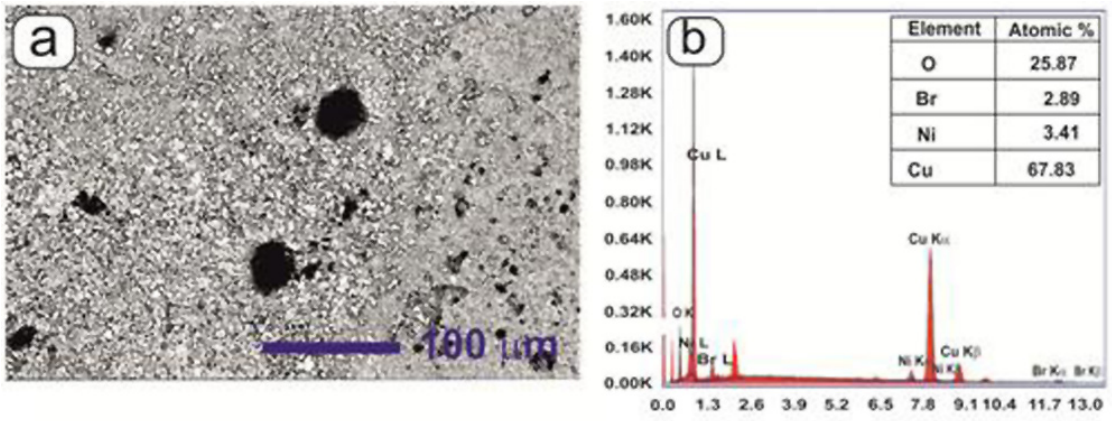

Fig. 7. SEM at 1000x (a) and EDX (b) after treated Cu/10 Ni in 5x10^{-1} M LiBr at constant potential of 900 mV (SCE) for 120 min.

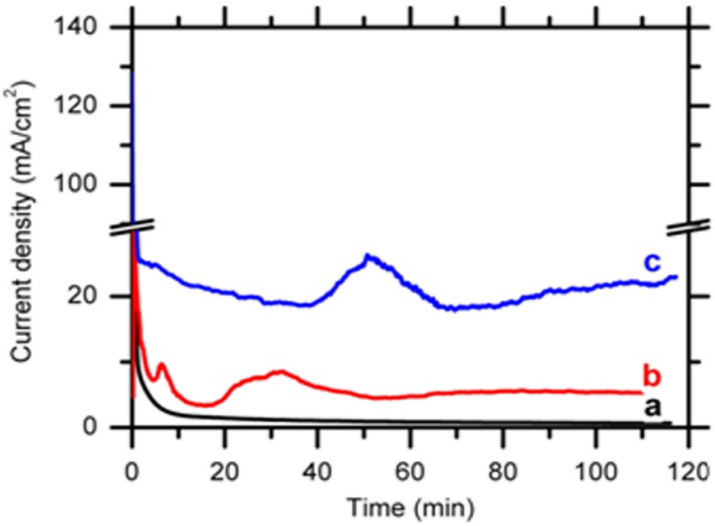

Fig. 8. Chronoamperometric curves of Cu/30 Ni in 3x10^{-1} M for 120 min at different potential values of (a) 150 mV, (b) 800 mV, and (c) 1600 mV. (all potentials were vs. SCE).

Further increase in the applied constant potential to 1600 mV, which represented what, happened after the breakdown at more anodic potential which is not yielding any hysteresis loop area as shown in Fig. 3b.

The current-time curve of Fig. 8c clarifies that after decrease the current from 25 to 19 mA.cm^{-2} at 40 min, the current density increased rapidly again to 26 mA.cm^{-2} through 10 min. that decrease again to nearly the same lower value and finally a

slightly increase in the current density value to 22 $mA.cm^{-2}$ at the end of the experiment. The SEM of Fig. 11a confirms the above results of current-time which shows that some of the film formed, especially around the edges of the sample, is peeled-up from the alloy surface at these locations to become bare to contact with LiBr solution. Figure 11b represented that there is no pitting attack and the region of the peeled-up film can be blocking with the reformed film of partial passive. The EDX analysis (Fig. 11c and 12) also confirmed the formation of partial passive film of $Cu_2(OH)_3Br$ and satisfy the denickelification phenomenon.

As increasing the concentration of LiBr to 5x 10^{-1} M, the same results recorded at $3x10^{-1}$ M were produced except as recorded in Fig. 3d where the partial passive region recorded at $5x10^{-1}$ M that started to appear at 400 mV and extended to 2000 mV is disappeared at 3 $x10^{-1}$ M LiBr. In 5 $x10^{-1}$ M LiBr the current density of Cu/30 Ni after 400 mV is increased as increasing the potential with higher rate and the partial passive current was recorded. This occurs as a result of the competition between the formation of the partial passive film and the dissolution of the alloy which tends to the higher dissolution at $5x10^{-1}$ M through the non-protective film formed.

The SEM of Fig. 13 (a, b) and Fig. 14 (a, b) shows that the surface covered with a non homogenous and non protective film. The EDX analysis of Figs. 13c and 14c represented clearly the formation of $Cu_2(OH)_3Br$ in soluble complex. Fig. 14c recorded a higher atomic conc. % of Br^- of 23.34 which is satisfying the deleterious effect of Br^- at this higher positive potential of 800 mV. At these values of potentials the surface of the alloy suffered from denickelification.

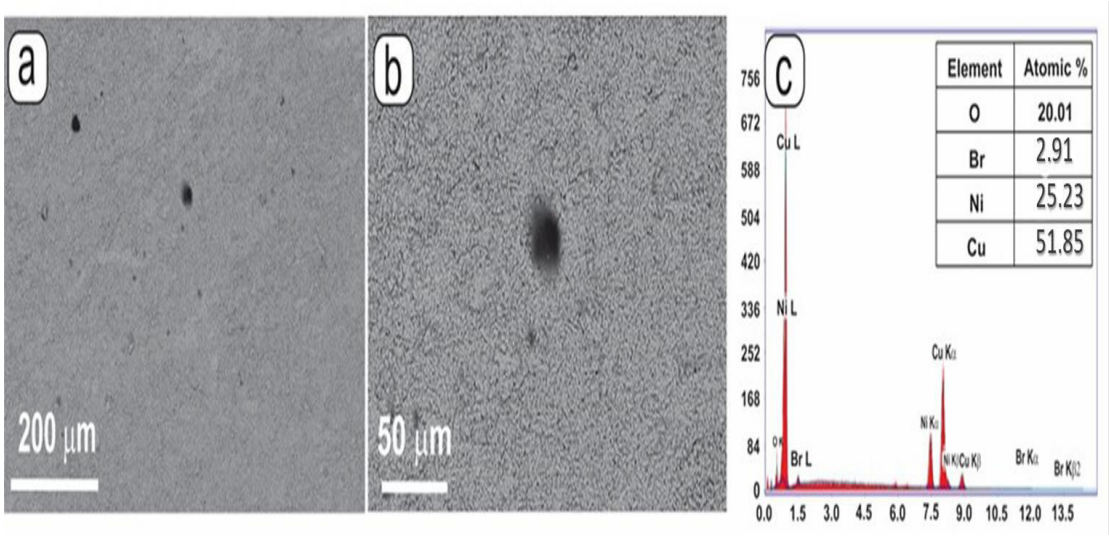

Fig. 9. SEM at 500x (a), 1500x (b) and EDX (c) after Cu/30 Ni treated in $3x10^{-1}$ M LiBr at a constant potential of 150 mV (SCE) for 120 min.

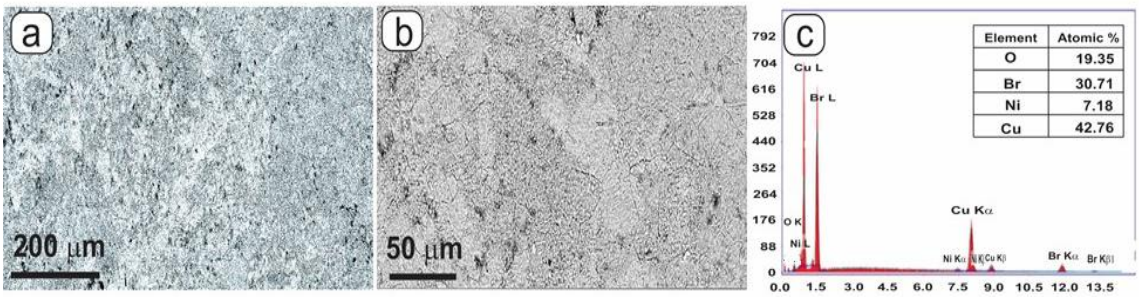

Fig. 10. SEM at 500x (a), 1500x (b) and EDX (c) of Cu/30 Ni after being treated in 3 $x10^{-1}$ M LiBr at constant potential of 800 mV (SCE) for 120 min.

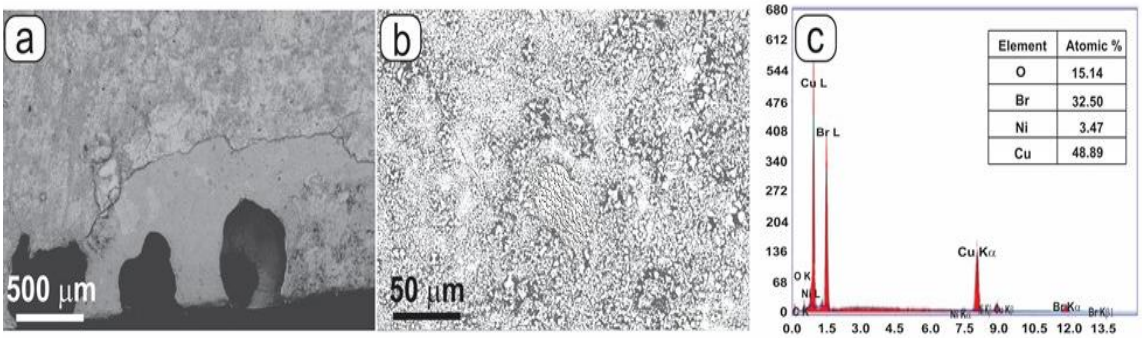

Fig. 11. SEM at 150x (a), 1500x (b) and EDX (c) of Cu/30 Ni in 3x10^{-1} M LiBr at constant potential of 1600 mV (SCE) for 120 min.

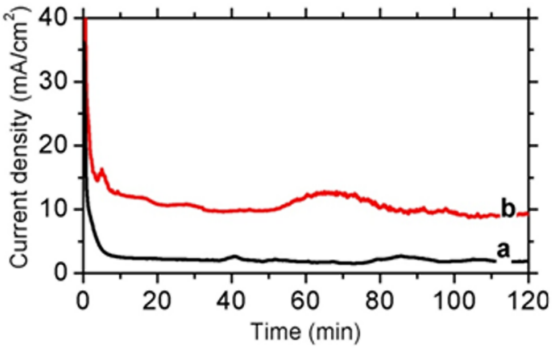

Fig. 12. Chronoamperometric curves of Cu/30 Ni in 5 x10^{-1} M LiBr at constant potentials of 300 (a) and 900 (b) for 120 min [All potentials were vs. SCE].

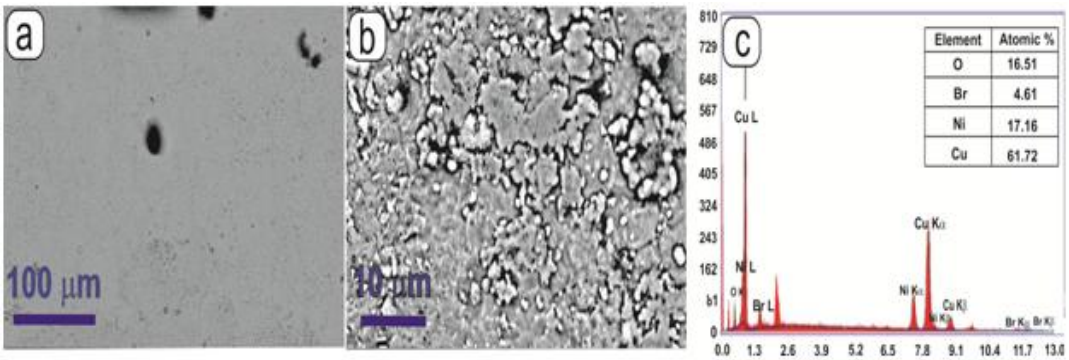

Fig. 13. SEM at 1000x (a), 8000x (b) and EDX (c) of Cu/30 Ni after being treated in 5x10^{-1} M LiBr at constant potential of 300 mV (SCE) for 120 min.

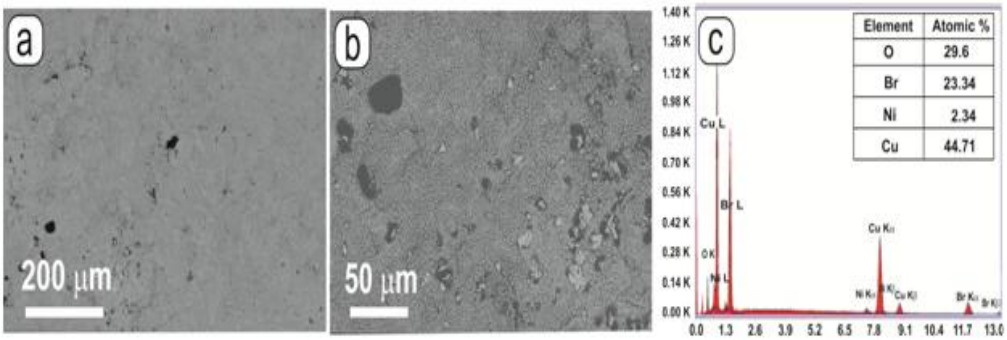

Fig. 14. SEM at 500x (a), 1500x (b) and EDX (c) of Cu/30 Ni after being treated in 5x10^{-1} M LiBr at constant potential of 800 mV (SCE) for 120 min.

Conclusions

1. The anodic potentiodynamic cyclic polarization showed that the corrosion potential shifted towards more negative values as increasing LiBr concentration. Two anodic peaks (P1, P2) appeared at ≤ $5x10^{-1}$ M LiBr. P1 is formed as a result of oxidation of Cu metal to CuBr and or Cu_2O while P2 is formed due to oxidation of Cu^+ to CuO and or $Cu(OH)_2$.

2. At higher concentration of LiBr ≥ 1 M, P2 disappeared as a result of the deleterious effect of Br^- on copper oxide to lose easily its passivity as soluble di-bromo cuprate complex ($CuBr_2^-$). At higher concentration of LiBr ≥ 1 M and at higher potential of ≥ 600 mV, Cu (I) acts on the simultaneous oxidation of Cu (I) to Cu (II) and reduction of Cu (I) to form metallic Cu on the electrode surface.

3. The passive current, the breakdown potential and the hysteresis loop started to appear at 0.1 M LiBr up to 1 M which disappeared at 2 M in case of Cu/10 Ni while in case of Cu/30 Ni they started to appear at 2 M which then disappeared at 6 M.

4. The current densities recorded are partially passive current of 2-5 $mA.cm^{-2}$. This occurred because the dissolution of the minor elements (dealloying).

5. In case of Cu/10 Ni at $5x10^{-1}$ M LiBr, two breakdown potentials, which yielded two hysteresis loops, the first one observed at 700 mV and the second one was observed at more anodic potential. While in case of Cu/30 Ni, pitting corrosion was manifested at 2 and 4 M LiBr only.

6. Chronoamperometric measurements proved that in case of Cu/10 Ni, in $5x10^{-1}$ M LiBr at constant potential of 300 mV, small current density of 2 $mA.cm^{-2}$ in comparison with that observed at constant potential of 900 mV. Examination of the surface at 300 mV showed that the surface was covered with a non-porous and homogeneous protective film of doped Cu_2O. On the other hand, pitting corrosion was detected at constant potential of 900 mV. The surface suffered from denickelification at the two values of applied constant potentials of 300 and 900 mV.

7. The very small current density recorded at 150 mV in case of Cu/30 Ni in $3x10^{-1}$ M LiBr is due to the formation of a doped protective Cu_2O and the surface analysis recorded an enrichment of Ni. As increasing the applied potential to 900 mV at the same condition, the surface analysis confirmed the formation of a non-protective film of $Cu_2(OH)_3Br$ and a higher value of Br^- detected is due to the autocatalytic dissolution and or the deleterious effect of the Br^-at higher applied constant potential of 900 mV. As increasing the concentration of LiBr to $5x10^{-1}$ M, nearly the same result obtained in case of using $3x10^{-1}$ M LiBr are produced and the surface suffered from the denickelification at all potentials and concentrations studied.

References

1. de Chazournes, L. B. Kyoto protocol to the united nations framework convention on climate change, UN's Audiovisual Library of International Law (http://untreaty. un. org/cod/avl/ha/kpccc/kpccc. html), (1998).

2. A. C. United Nations Environment Programme. Refrigeration, H.P.T.O. Committee, Montreal protocol on substances that deplete the ozone layer, UNEP, (1994).

3. Labus, J. M., Bruno, C. J., Coronas, A. Review on absorption technology with emphasis on small capacity absorption machines. *Thermal Science*, **17**, 739-762 (2013).

4. Guiñón, J. L., García-Antón, J., Pérez-Herranz, V., Lacoste, G. Corrosion of carbon steels, stainless-steels, and titanium in aqueous lithium bromide solution. *Corrosion*, **50**, 240-246 (1994).

5. Leiva-Garcia, R., Muñoz-Portero, M. J., García-Antón, J., Sánchez-Tovar, R. Effects of hydrodynamic conditions and LiBr concentration on the corrosion of copper in LiBr absorption machines. *Int. J. Electrochem. Sci.* **7**, 1332-1347 (2012).

6. Cuevas-Arteaga, C., Concha-Guzmán, M. O. Corrosion study of SS-316L exposed to LiBr-H_2O solution applying electrochemical techniques and weight loss method. *Corros. Eng. Sci. Techn.* **44**, 57-68 (2009).

7. Abd El Meguid, E. A., Abd El Rehim, S. S., Al Kiey, S. A. Inhibitory effect of cetyltrimethyl ammonium bromide on the corrosion of 904L stainless steel in LiBr solution. *Corros. Eng. Sci. Techn.* **51**, 429-437 (2016).

8. Arteaga, C. C., Calderón, J. P., Sedano, C. F. C., Rodríguez, J. A. Comparison of corrosion resistance of carbon steel and some stainless steels exposed to LiBr-H_2O solution at low temperatures.

Int. J. Electrochem. Sci. **7**, 445-470 (2012).

9. Hu, X. Q., Liang, C. H., Wu, X. N. Corrosion behaviors of carbon steel in 55% LiBr solution containing PWVA inhibitor. *Mater. Corros.* **62**, 444-448 (2011).

10. Liang, C. H., Hu, X. Q., Ma, L. Effects of Na3PW12O40 on the corrosion behavior of carbon steel in 55% LiBr solution. *Mater. Corros.* **58**, 39-43 (2007).

11. Li, J. L., Liang, C. H., Huang, N. B. Effect of B-Mo-W complex inhibitor on corrosion of mild steel in 55% LiBr solution. *J. Mater. Eng. Perform.* **24**, 4456-4461 (2015).

12. Fernández-Domene, R. M., Blasco-Tamarit, E., García-García, D. M., Antón, J. G. Passivity breakdown of titanium in LiBr Solutions. *J. Electrochem. Soc.* **161**, C25-C35 (2014).

13. Fernández-Domene, R. M., Blasco-Tamarit, E., García-García, D. M., García-Antón, J. Cavitation corrosion and repassivation kinetics of titanium in a heavy brine LiBr solution evaluated by using electrochemical techniques and Confocal Laser Scanning Microscopy. *Electrochim. Acta,* **58**, 264-275 (2011).

14. Goidanich, S., Brunk, J., Herting, G., Arenas, M., Wallinder, I. O. Atmospheric corrosion of brass in outdoor applications: Patina evolution, metal release and aesthetic appearance at urban exposure conditions. *Science of the total environment*, **412**, 46-57 (2011).

15. la Fuente, D. De, Simancas, J., Morcillo, M. Morphological study of 16-year patinas formed on copper in a wide range of atmospheric exposures. *Corros. Sci.* **50**, 268-285 (2008).

16. Druska, P., Strehblow, H. -H., Golledge, S. A surface analytical examination of passive layers on CuNi alloys: Part I. Alkaline solution. *Corros. Sci.* **38**, 835-851 (1996).

17. Druska, P., Strehblow, H. -H. Surface analytical examination of passive layers on Cu-Ni alloys part II. Acidic solutions. *Corros. Sci.* **38**, 1369-1383 (1996).

18. Powell, C. A. Copper-nickel sheathing and its use for ship hulls and offshore structures. *International biodeterioration & biodegradation*, **34**, 321-331 (1994).

19. Alfantazi, A., Ahmed, T., Tromans, D. Corrosion behavior of copper alloys in chloride media. *Mater Design*, **30**, 2425-2430 (2009).

20. Kato, C., Pickering, H. A Rotating Disk Study of the corrosion behavior of Cu-9.4 Ni-1.7 Fe alloy in Air-Saturated aqueous NaCl solution. *J. Electrochem. Soc.* **131**, 1219-1224 (1984).

21. Kato, C., Castle, J., Ateya, B. , Pickering, H. On the mechanism of corrosion of Cu-9.4 Ni-1.7 Fe alloy in air saturated aqueous NaCl solution II. composition of the protective surface layer. *J. Electrochem. Soc.* **127**, 1897-1903 (1980).

22. Metikoš-Huković, M., Babić, R., Škugor, I., Grubač, Z. Copper–nickel alloys modified with thin surface films: corrosion behaviour in the presence of chloride ions. *Corros. Sci.* **53**, 347-352 (2011).

23. El Meleigy, A. E., Abd Elhamid, Sh. E., El Warraky, A. A. Corrosion behaviour of copper in LiBr solutions- surface examination. *Materwiss. Werksttech.* **46**, 59-68 (2015).

24. El Meguid, E. A. A., Awad, N. K. Electrochemical pitting corrosion behaviour of α-brass in LiBr containing solutions. *Corros. Sci.* **51**, 1134-1139 (2009).

25. Lee, C. K., Shih, H. C. Effect of halide ions on electrochemical behavior and stress corrosion cracking of 67/33 α-brass in aqueous environments. *Corrosion*, **52**, 690-696 (1996).

26. Youssef, G. I., El Meleigy, A. E., Khorshed, L. A., Attia, A., Ashour, E. A. Inhibitive effect of benzotriazole on the corrosion and corrosion fatigue of α-Al bronze alloy in LiBr solution. *Materials and Corrosion*, **69**, 1827-1836 (2018).

27. Fenelon, A. M., Breslin, C. B. An electrochemical study of the formation of benzotriazole surface films on copper, zinc and a copper-zinc alloy. *J. Appl. Electrochem.* **31**, 509-516 (2001).

28. Kosec, T., Merl, D. K., Milošev, I. Impedance and XPS study of benzotriazole films formed on copper, copper-zinc alloys and zinc in chloride solution. *Corros. Sci.* **50**, 1987-1997 (2008).

29. Ramirez-Arteaga, M. A. , Gonzalez-Rodriguez, J. G., Rosales, I. , Dominguez-Patiño, G., Martinez-Villafañe, A., Neri-Florez, M. A. Corrosion inhibition of 70Cu-30Ni alloy in LiBr plus ethylene glycol + H_2O mixtures by inorganic compounds. *Mater. Corros.* **62**, 41-46 (2011).

30. El Warraky, A. A., El Meleigy, A. E., Abd El Hamid, Sh. E. The electrochemical behaviour of 70-30 Cu-Ni alloy in LiBr solutions. *EJCHEM*, **59**, 833-850 (2016).

31. Muñoz, A. I., Antón, J.G., Guiñón, J. L., Herranz, V. P. Comparison of inorganic inhibitors of copper, nickel and copper-nickels in aqueous lithium bromide solution. *Electrochim. Acta,* **50**, 957-966 (2004).

32. Igual-Muñoz, A., García-Antón, J., Guiñón, J., Pérez-Herranz, V. Galvanic study of zinc and copper in lithium bromide solutions at different temperatures. *Corrosion*, **57**, 516-522 (2001).

33. Itzhak, D., Greenberg, T. Galvanic corrosion of a copper alloy in lithium bromide heavy brine environments. *Corrosion*, **55**, 795-799 (1999).

34. Muñoz, A. I., Antón, J. G., Guiñón, J., Herranz, V. P. Galvanic studies of copper coupled to alloy 33 and titanium in lithium bromide solutions. *Corrosion*, **58**, 995-1003 (2002).

35. Muñoz, A. I., Antón, J. G., Guiñón, J., Herranz, V. P. Corrosion behavior and galvanic studies of brass and bronzes in aqueous lithium bromide solutions. *Corrosion*, **58**, 560-569 (2002).

36. Muñoz-Portero, M. J., García-Antón, J., Guiñón, J. L., Perez-Herranz, V. Corrosion of copper in aqueous lithium bromide concentrated solutions by immersion testing. *Corrosion*, **62**, 1018-1027 (2006).

37. Aben, T., Tromans, D. Anodic polarization behavior of copper in aqueous bromide and bromide/benzotriazole solutions. *J. Electrochem. Soc.* **142**, 398-404 (1995).

38. El Meleigy, A. E., Shehata, M. F., Youssef, G. I., Elhamid, Sh. E., El Warraky, A. A. Role of Li^+ on the pitting corrosion of copper in LiBr solutions. *Ochrona przed korozją*, **55**, 427-431 (2012).

39. El Meleigy, A. E., Elhamid, Sh. E., El Warraky, A. A. Corrosion behaviour of copper in LiBr solutions: Effect of temperature. *British Journal of Applied Science & Technology*, **11**, 1-18 (2015).

40. El warraky, A. A. Dissolution of brass 70/30 (Cu/Zn) and its inhibition during the acid wash in distillers. *J. Mater Sci.* **31**, 119-127 (1996).

41. Abd Elhamid, Sh. E. Corrosion behaviour of copper and some of its alloys in LiBr solutions. *MSc. Thesis*, Ain Shams University, Cairo, Egypt. (2013).

42. Muñoz-Portero, M., García-Antón, J., Guiñón, J. , Pérez-Herranz, V. Pourbaix diagrams for nickel in concentrated aqueous lithium bromide solutions at 25°C. *Corrosion*, **63**, 625-634 (2007).

43. El Warraky, A. A., El Shayeb, H., Sherif, E. Electrochemical behaviour of Copper in Sodium bicarbonate solutions. Egypt. *J. Chem.* **47** (2004).

44. El Warraky, A. A., El Shayeb, H., Sherif, E. Pitting corrosion of copper in chloride solutions. *Anti-corrosion Methods and Materials*, **51**, 52-61 (2004).

سلوك التآكل لسبائك النحاس -النيكل في محاليل بروميد الليثيوم : دراسة مقارنة

شيماء عصمت عبد الحميد[١]، عبير عصمت المليجى[١]، عادل عطية[١]، علي عبد الفتاح الوراقى[١]، سعد محمد عبد الوهاب[٢]

[١] قسم الكيمياء الفيزيقية - المركز القومى للبحوث - الجيزة - مصر.

[٢] قسم الكيمياءالفيزيائية , كليه العلوم , جامعة عين شمس , عباسية - القاهرة -مصر.

تمت دراسة الاستقطاب الحلقى البتنشيوديناميكى لكلا من سبيكة النحاس ١٠ نيكل و ٣٠ نيكل فى محاليل ذات تركيزات مختلفة من بروميد الليثيوم من ١٠-١ إلى ٩ مولر. قد تبين من الدراسة حدوث انهيار للجهد وحلقة هستيرية وحماية للتيار بقيم اعلى فى حالة سبيكة النحاس ١٠ نيكل بالمقارنة بالنحاس ٣٠ نيكل . كما اظهرت كثافة التيار قيمة اعلى خلال اللحظات الاولى من استقطاب السبيكة كنتيجة للتغيرات التى تحدث على السطح. عند تركيز ٥×١٠-١مولر لسبيكة النحاس ١٠ نيكل وجد قيمتين لجهد الانهيار ونتج عنه حلقتين هستريتين احدهما عند ٧٠٠ ملى فولت والثانية عند جهد انودى اكثر ولم تسجل هذه الحالة فى حالة النحاس ٣٠ نيكل بينما ظهر تآكل نقرى عند تركيز ٢, ٤ مولر من بروميد الليثيوم . كما اوضحت قياسات التيار مع الزمن والفحص السطحى للسبيكتين انه فى حالة النحاس ٣٠ نيكل عند تركيزات ٣×١٠-١, ٥×١٠-١مولرعند جهد انودى اقل (١٥٠ملى فولت) بداية تكون عدد صغير من النقر محاط بطبقة حماية من Cu_2O ووجود النيكل بنسبة عالية على السطح. (enrichment of nickel)بينما فى كل حالات الجهد التى تمت دراستها لكل من نحاس ١٠ نيكل و النحاس ٣٠ نيكل عانى من نقص النيكل على السطح (denickelification).